inorganics

MDPI

Article

Cyanoguanidine-Modified Chitosan as an Efficacious Adsorbent for Removing Cupric Ions from Aquatic Solutions: Kinetics, Isotherms, and Mechanisms

Ard elshifa M. E. Mohammed [1,*], Nouf F. Al-Harby [1], Muneera Alrasheedi [1], Shaimaa M. Ibrahim [2] and Nadia A. Mohamed [1,*]

[1] Department of Chemistry, College of Science, Qassim University, Buraidah 51452, Saudi Arabia; hrbien@qu.edu.sa (N.F.A.-H.); mu.alrasheedi@qu.edu.sa (M.A.)
[2] Department of Chemistry, Faculty of Education, Ain Shams University, Roxy, Cairo 11711, Egypt; shimaaabdelaal@edu.asu.edu.eg
* Correspondence: ar.mohamed@qu.edu.sa (A.e.M.E.M.); na.ahmed@qu.edu.sa (N.A.M.)

Abstract: One of the most critical environmental needs is to remove metal ions from industrial wastewater. In this investigation, chitosan modified by cyanoguanidine (CCs) was employed for the first time to adsorb cupric ions. The optimal conditions for eliminating cupric ions were adsorbent dose = 0.015 g, cupric ion concentration = 0.2 g L^{-1}, pH = 6, and temperature = 25 °C. The adsorption kinetics fit the pseudo-second-order model, showing a value of correlation coefficient (R^2) of 1.00, which is the highest. The experimental q_e value was determined to be 99.05 mg g^{-1}, which is comparable to 100 mg g^{-1} (the theoretical one). The adsorbent's removal efficacy was 96.05%, and the adsorption isotherms, which conform to the Freundlich model, show that adsorption is multi-layered and homogeneous. The chemosorption and physisorption processes are major factors in the elimination of copper ions. Therefore, a good approach to generate an appropriate efficient adsorbent, which is a good alternative approach in cupric ion elimination, is to incorporate cyanoguanidine, which possesses additional binding sites for cupric ions between chitosan chains. Further, the mechanism of Cu^{2+} adsorption onto CCs was proposed on the basis of FTIR analysis and computational studies.

Keywords: chitosan; cyanoguanidine; cupric ions; adsorption studies; kinetics; isotherms

check for updates

Received: 25 January 2025
Revised: 20 March 2025
Accepted: 3 April 2025
Published: 6 April 2025

Citation: Mohammed, A.e.M.E.; Al-Harby, N.F.; Alrasheedi, M.; Ibrahim, S.M.; Mohamed, N.A. Cyanoguanidine-Modified Chitosan as an Efficacious Adsorbent for Removing Cupric Ions from Aquatic Solutions: Kinetics, Isotherms, and Mechanisms. *Inorganics* **2025**, *13*, 116. https://doi.org/10.3390/inorganics13040116

Copyright: © 2025 by the authors. Licensee MDPI, Basel, Switzerland. This article is an open access article distributed under the terms and conditions of the Creative Commons Attribution (CC BY) license (https://creativecommons.org/licenses/by/4.0/).

1. Introduction

Pollution by heavy metals is recognized as a critical issue for ecosystems worldwide, particularly for aquatic resources [1]. As they move through the food chain, they build up in aquatic plants' and animals' biological systems, presenting a significant danger to their health [2]. The effluents and wastes from various industries, like steel, fertilizer, electroplating, printing, and mining, can introduce heavy metals into ecosystems [1]; they can also enter through mining activities, dye manufacturing, plant disease control agent synthesis, the erosion of soil, and the process of the natural weathering of the crust of the Earth [3]. Assorted techniques, such as membrane filtration [1,4], ion exchange [5], chemical precipitation [6], and activated carbon adsorption [7], have been employed to reduce heavy metal ion concentrations in water [8].

Although these methods are all efficient, they are constrained by various factors, such as high energy usage, expensive costs, potentially dangerous byproducts from reagents, and inadequate outcomes with low metal concentrations. Researchers are showing a lot of

interest in the biosorption process, as it is considered a superior option. Key characteristics of biosorption include efficiency, user-friendly design, simplicity, quick operation, low operating expenses, lack of undesirable outcomes, eco-friendliness, numerous adsorbents, and simple regeneration for future reuse [9].

Many metals in the fourth period of the periodic table can lead to cancer. The assumption is that the electronic configuration of these transition metals is the main cause of this carcinogenicity [10]. Issues occur when there is too much or too little copper, as it is essential for numerous enzymes in all types of organisms [9]. Copper is one of the most frequently utilized heavy metals. Many organisms are harmed by cupric ions, which are commonly present in the environment [11–13]. Specific actions, like using copper-lined or -painted pots for cooking and copper pipes for water supply, can lead to the exposure of human beings to dangerously elevated amounts of harmful copper in their food and drinking water [8,14]. Furthermore, copper sources in sewage effluent include waste from mining and fertilizer industries, as well as waste from baths with copper paints, pigments, and plating [15]. An excess of copper in water can lead to harmful consequences, such as neurotoxicity, liver and kidney failure, jaundice, respiratory issues, diarrhea, and ultimately possible death, despite the fact that organisms only need a small amount of copper [16–19]. A key epidemiological discovery indicating that copper may be a main cause of cancer is the high rate of cancer among coppersmiths [9]. According to both the USA Environmental Protection Agency (EPA) and the World Health Organization, the allowed range for copper in drinking water is between 1.3 and 2.0 mg/L [20].

Due to the antibacterial properties of the biopolymer chitosan [21,22], together with its capacity for metal adsorption [23,24] and its capability to uptake acidic dyes [25,26], it has become increasingly valuable in the field of biotechnology in relation to environmental concerns. Additionally, chitosan is abundant, sustainable, biocompatible, biodegradable, and hydrophilic [8,27].

The high solubility of chitosan in acids is seen as a major drawback, particularly when it is utilized in industrial wastewater treatment to adsorb pollutants, which often have an acidic nature. Hence, it is crucial to control the solubility of chitosan for such applications. Graft copolymerization [28,29], the blending of polymers [30], and chemical substitution [31] are the techniques employed to achieve this target. Also, chitosan can be chemically cross-linked to improve its mechanical properties, increase its chemical stability in acidic solutions, delay its deterioration, and extend its shelf life in diverse environments, making it a suitable alternative [32,33].

Polyacrylonitrile grafted with chitosan has been employed to remove copper. Copper absorption was consistent to both the pseudo-second-order and Langmuir models. The best parameters were pH = 7.5, 5 g of adsorbent, and an equilibrium time of 5–6 h. Adsorption capacity reached a maximum of 239.314 mg g^{-1} [34]. Chitosan-coated $MnFe_2O_4$ nanoparticles effectively eliminated low levels of harmful cupric ions (22.6 mg g^{-1}) [35]. pH 5 resulted in cotton gauze coated with chitosan being able to absorb a maximum of 14.4 mg g^{-1} of Cu(II) ions. Moreover, as the metal ion concentration increased, the removal efficiency decreased, while the adsorption process remained unaffected by temperature [36]. Another study reported that the highest adsorption capacity for Cu (II) at 328 K was 139.797 mg g^{-1}, using xanthate modified by magnetic chitosan-crosslinked poly(vinyl alcohol) [37]. At a pH of 4, the chitosan beads crosslinked and grafted with poly(methacrylamide) showed an optimal adsorption capacity of 140.9 mg g^{-1} for cupric ions [38]. Under optimal conditions, the beads of chitosan and poly(vinyl alcohol) blends modified using poly(ethylene glycol) achieved a 99.99% adsorption rate. These conditions included a pH of 5, a temperature of 45 °C, a 5 h equilibrium time, 1 g L^{-1} of adsorbent, and a 25 mg L^{-1} cupric ion concentration [39]. A distinguished adsorption capability of

cupric ions was observed in cross-linked chitosan modified with polyaniline, achieving 131.58 mg g^{-1} at 40 °C, pH 6, and an initial concentration of 100 mg L^{-1} [40].

Guanidine-based derivatives are capable of binding to metals. Cyanoguanidine is a nitrogen-rich organic substance that possesses a guanidine moiety and a cyano group bonded to one of its nitrogen atoms. The guanidinylation of carboxymethyl chitosan is considered to be one of the most effective processes to improve its adsorption capacity of metal ions and dyes for industrial wastewater treatment [41,42].

Thus, it would be expected that the inclusion of nitrogen-rich cyanoguanidine moieties as cross-linkages between the chains of chitosan, in addition to the regained amino groups of chitosan, will increase the binding sites available for the adsorption of Cu(II) ions. Further, the cross-linking of chitosan using cyanoguanidine will improve its properties, in addition to increasing its functionality, such as lowering of its solubility, inhibiting its degradation rate, increasing the life span of its products in different media, and consequently promoting its easy restoration and regeneration for reuse.

Accordingly, chitosan, which was modified with cyanoguanidine (CCs) in our previous research study [42], was utilized for the first time in this work as an adsorbent to eliminate cupric ions from aqueous solutions. Both the isotherms and kinetics of the adsorption process of cupric ions onto cyanoguanidine-modified chitosan were studied. Furthermore, the current work was extended to investigate the impacts of certain variables that control the adsorption process, including the quantities of both the adsorbent and cupric ions, pH values, temperatures, and time periods. The mechanism of Cu^{2+} adsorption onto CCs was also suggested based on FTIR analysis and computational studies.

2. Results and Discussion

2.1. Characterization of CCs Adsorbent

2.1.1. FTIR Analysis

The FTIR spectra of chitosan and its modified derivatives are demonstrated in Online Supplementary Figure S1. In the spectrum of chitosan, the existence of saccharide moieties was confirmed by the appearance of four absorption peaks at 1158, 1074, 1029, and 894 cm^{-1}. A dense broad absorption peak at around 3700 to 3000 cm^{-1} appeared, relating to the stretching vibration of -OH groups that overlapped with that of -NH_2 and their hydrogen bonds. Symmetric absorption peaks corresponding to the -CH and -CH_2 groups in the pyranose rings appeared at 2924 and 2864 cm^{-1}, respectively. The high extent of deacetylation of chitosan was confirmed by the appearance of two weak absorption peaks at 1658 and 1593 cm^{-1}, assigned to amide I and amide II, respectively. The overlapping between the amino groups' deforming vibration at 1600 cm^{-1} and the stretching vibration peak of amide I at 1658 cm^{-1} resulted in an intensive peak [43,44].

The spectrum of chitosan Schiff's base displayed similar absorption peaks to chitosan in addition to some new peaks, as follows: (1) 3052 and 3027 cm^{-1}, indicated to C-H groups in the aromatic ring; (2) 1691 cm^{-1}, corresponding to C=N groups; (3) 1600, 1579, 1493, and 1454 cm^{-1}, related to the C=C bond in the aromatic rings; and (4) 757 and 692 cm^{-1} (strong) due to the mono-substituted benzene rings [42].

The epoxy chitosan Schiff's base spectrum, in addition to the afore-mentioned peaks, displayed a new peak at 1250 cm^{-1} due to the epoxide moieties [45].

The spectrum of cyanoguanidine chitosan Schiff's base showed that the disappearance of the peak corresponded to the epoxide linkages at 1250 cm^{-1}, and the appearance of two new peaks at 2207 and 2162 cm^{-1} related to the C≡N group of the cyanoguanidine moiety [46], indicating the occurrence of the interaction between the epoxide rings and the NH_2 groups of cyanoguanidine. Moreover, the stretching vibration peak corresponding to the C=N group of the cyanoguanidine moiety appeared at 1641 cm^{-1}.

The removal of benzaldehyde moieties to obtain CCs adsorbent was confirmed by the disappearance of the absorption bands of the mono-substituted benzene ring at 757 and 692 cm^{-1}.

2.1.2. XRD Analysis

Unlike chitosan, the modified derivatives exhibited reduced crystallinity due to a decrease in the hydrogen bonds between their chains (Online Supplementary Figure S2). This was shown by the vanishing of the peak at $2\theta = 10^0$ and the weakening of the peak at $2\theta = 20^0$. Chitosan's functionality was drastically changed after this modification because the polar $-NH_2$ and/or -OH groups were consumed, in addition to the incorporated modifiers' moieties that kept the modified chitosan chains apart from one another.

2.1.3. SEM Analysis

The rough texture provided by the equally dispersed lumps with varying sizes on the surfaces of the modified chitosan derivatives relative to the smooth texture of chitosan is shown in Online Supplementary Figure S3. This indicates that all chitosan modification steps were completed successfully, creating a porous matrix with a large surface area by separating the modified chitosan chains and reducing the formation of their hydrogen bonds.

2.2. pHzpc

pHzpc is the pH value at which the total charges on the surface equal zero in certain temperature and aqueous solution composition circumstances. The surface at pHpzc has an equal amount of positive and negative charges, which is not to indicate that there are not any. The solution pH and type, as well as the number of functional groups, all influence the amount of the surface charges. pHzpc is important for surface characterization because it indicates the ease with which an adsorbent may potentially bind hazardous ions. This is because, for pH values higher than pHzpc, the adsorbent surface has a net negative charge that encourages the adsorption of cationic species. On the other hand, the adsorbent rejects cations when the pH is lower than pHzpc because of the net positive charge of $-NH_2^+$ on its surface. For CCs, the pHzpc value was found to be 6.5 using the salt addition method (Figure 1). For pH augmentation, all the nitrogen and oxygen atoms along CCs retain their lone pairs of electrons and thus could efficaciously bind to metallic cations [47,48].

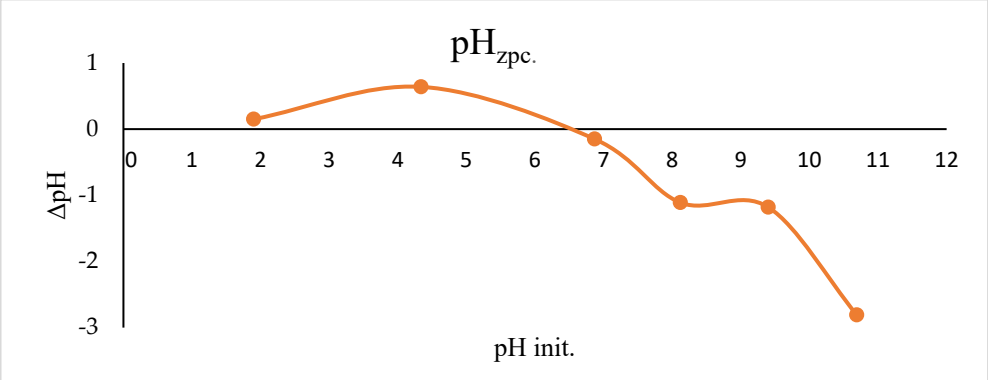


Figure 1. pHzpc plot for CCs.

2.3. Optimizing Adsorption

2.3.1. Effect of Cupric Ion Concentration

From Figure 2, it can be noted that the adsorption capacity of CCs ranged from 14.71 to 174.25 mg g^{-1} when the initial concentration of the cupric ion aqueous solution ranged between 20 and 200 mg L^{-1}. This may be ascribed to the fact that at low cupric ion

concentrations, there is only a small divide between the cupric ion amount and the overall number of attainable adsorption sites, resulting in partial adsorption. At high cupric ion concentrations, the adsorption capacity increases; this is attributed to the concentration gradient as a high driving force [42,49,50].

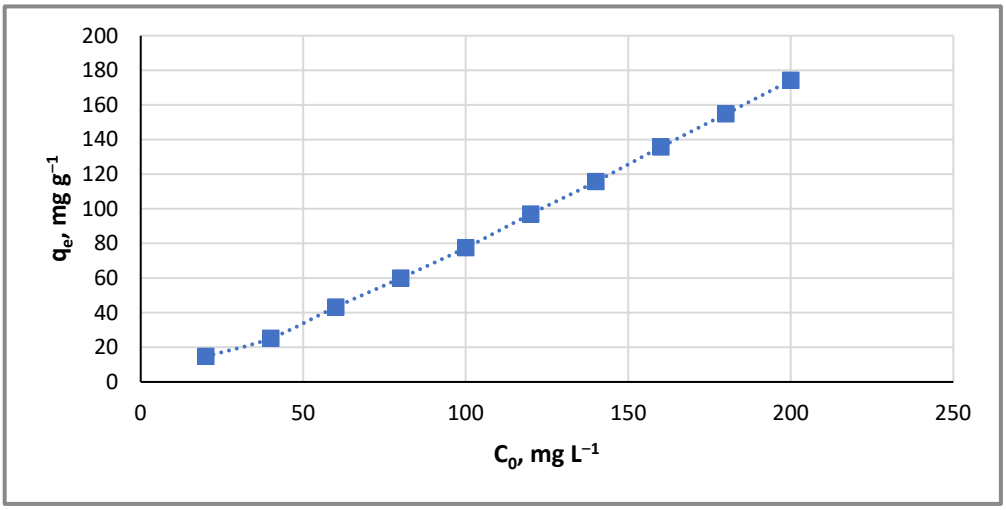


Figure 2. Effect of concentration of cupric ions on their adsorption by CCs.

2.3.2. Effect of Temperature

The results demonstrated a slight decrease in the percentage of cupric ion removal efficiency by CCs from 25 to 35 °C, as shown in Figure 3. The removal efficiency was 76.96% at 25 °C and 75.71% at 35 °C. This indicates that the elimination procedure is exothermic at this temperature range, where physicochemical adsorption dominates. However, as the temperature rose from 35 to 55 °C, the elimination efficiency increased mildly from 75.71 to 76.66% (Figure 3). This indicated that the elimination process in this stage was endothermic and occurred in a chemisorption manner. Due to the rise in temperature, cupric ions became increasingly mobile and gained enough energy to interact with the active sites of CCs. Additionally, the rise in the temperature resulted in a decrease in solution viscosity and an increase in the rate of cupric ion diffusion via the exterior frontier layer of the adsorbent. Furthermore, raising the reaction temperature allows for improving the penetration of cupric ions into the pores of CCs and enhances the removal efficiency percentage [51].

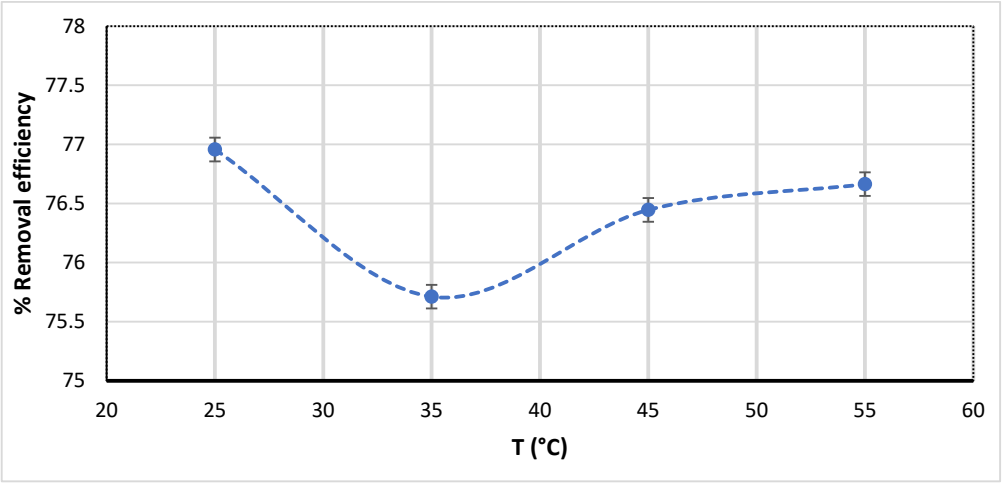


Figure 3. Effect of temperature on cupric ion removal by CCs.

2.3.3. Effect of Solution pH

A medium pH is essential for metal ion adsorption as it is related to the positive and negative surface charges of the adsorbent. The efficiency of the elimination of cupric ions by CCs was investigated using pH levels ranging from 1 to 6 to determine the effect of solution pH on their removal (Figure 4). Cupric ions precipitated as cupric hydroxide at pH $\geq$ 7. Previous studies found that the coagulation of metal ions is facilitated by ion exchange and electrostatic interactions at low and high pH, respectively [52,53]. The results showed that as the solution pH increased from 1 to 6, the removal efficiency increased from 76.44 to 96.05%, respectively. It is evident from these findings that the ion exchange mechanism was responsible for the increase in Cu^{2+} adsorption. At lower pH values, the competition for active sites on the adsorbent between H^+ and Cu^{2+} may be responsible for this behavior; H^+ ions are preferred for adsorption due to their smaller size compared to cupric ions. Increasing pH values from 4 to 6 (<pH_{zpc}) revealed a successive improvement in Cu^{2+} removal efficiency, reflecting the victory of Cu^{2+} in the contest against H^+ for coordination with the binding sites of the adsorbent.

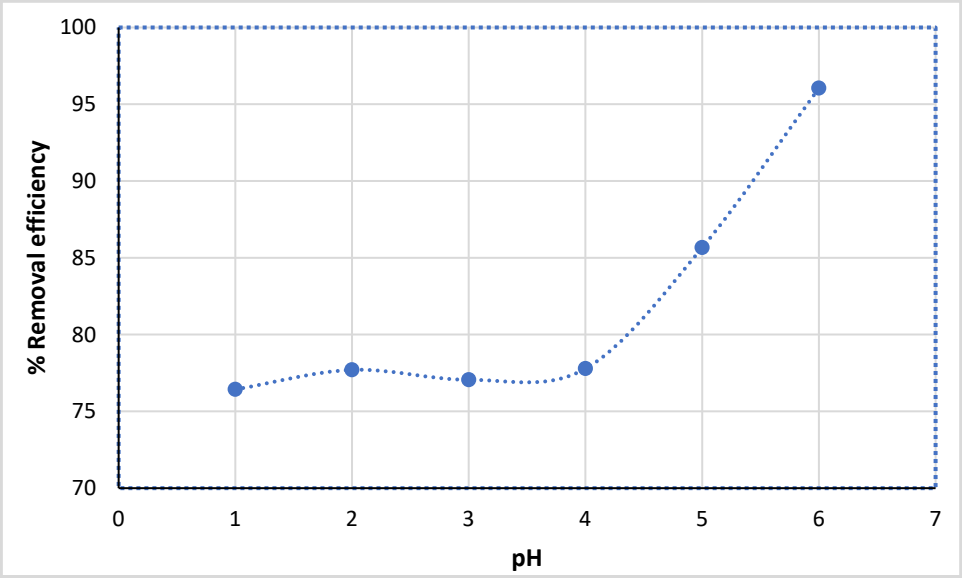
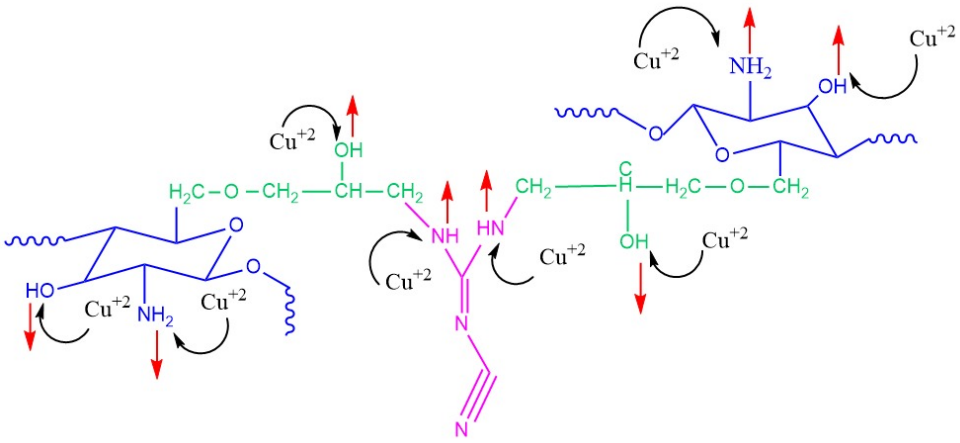


Figure 4. Effect of cupric ions' solution pH on their elimination using CCs.

The hypothetical cupric ion interactions and the functional groups on the CCs adsorbent (-OH, -NH_2, -NH) are shown in Scheme 1.



Scheme 1. A hypothetical representation of cupric ion adsorption onto CCs at pH 6.

2.3.4. Adsorbent Dosage Effect

Under constant conditions (volume of cupric ion solution = 10 mL, concentration = 100 mg L^{-1}, pH 4, at 25 °C for 24 h), various amounts of CCs (2–15 mg) were employed to identify the impact of CCs dose on the removal percent of cupric ions, as illustrated in Figure 5. The results show that the elimination rate of cupric ions using CCs increased from 77.51 to 81.22% by increasing the CCs dose from 2 to 15 mg. This may be attributed to the increases in adsorbent surface area, leading to more exchangeable binding sites available for the uptake of cupric ions as the adsorbent dosage increased [54–58].

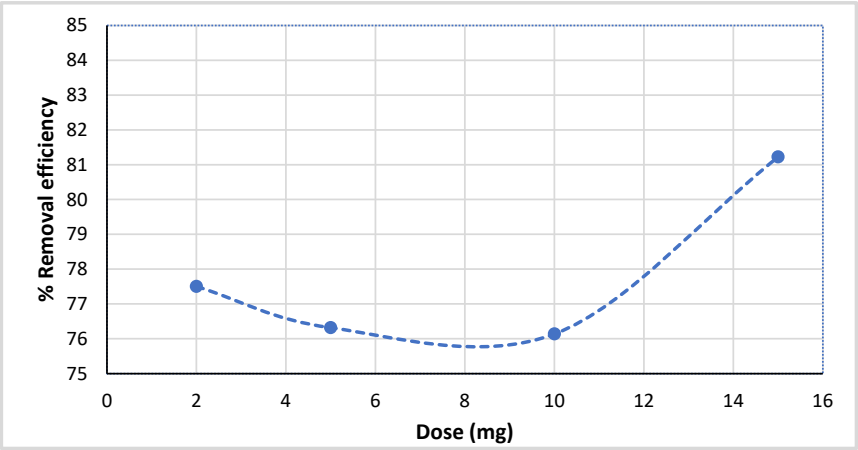


Figure 5. Effect of the CCs dose on elimination of cupric ions.

2.4. Adsorption Kinetics

Figure 6 shows the results of the adsorption kinetics of the cupric ions using 50 mg of CCs, 50 mL of cupric ion solution (100 mg L^{-1}), a temperature of 25 °C, and a solution pH of 6. Table 1 gives a summary of the variables of different kinetic models. The pseudo-second-order model showed the highest correlating coefficient value (R^2 = 1.00) among all the applied models (Table 1). So, we can undoubtedly assert that the pseudo-second-order model is capable of accurately describing the system. Additionally, the measured q_e value (99.05 mg g^{-1}) closely matches the theoretical one (100 mg g^{-1}), as shown in Table 1, demonstrating a significant agreement with the pseudo-second-order model. This is an evaluation and confirmation of how well the pseudo-second-order kinetic model accurately represents the adsorption of cupric ions by CCs.

Table 1. Correlation coefficients and constants of the adsorption kinetic models of cupric ions using CCs.

Kinetic Models	Parameters	
	$q_{e.exp}$ (mg g^{-1})	99.05
Pseudo-first-order	R^2	0.924
	$q_{e.cal}$ (mg g^{-1})	1.781
	k_1 (min^{-1})	0.023
Pseudo-second-order	R^2	1
	$q_{e,cal}$ (mg g^{-1})	100
	k_2 (10^{-5}) (g mg^{-1} min^{-1})	0.050
Elovich	R^2	0.91
	β (g mg^{-1})	0.975
	α (10^{39}) (mg g^{-1} min^{-1})	4.706
Intraparticle diffusion	R^2	0.919
	k (mg g^{-1} $min^{-1/2}$)	0.485

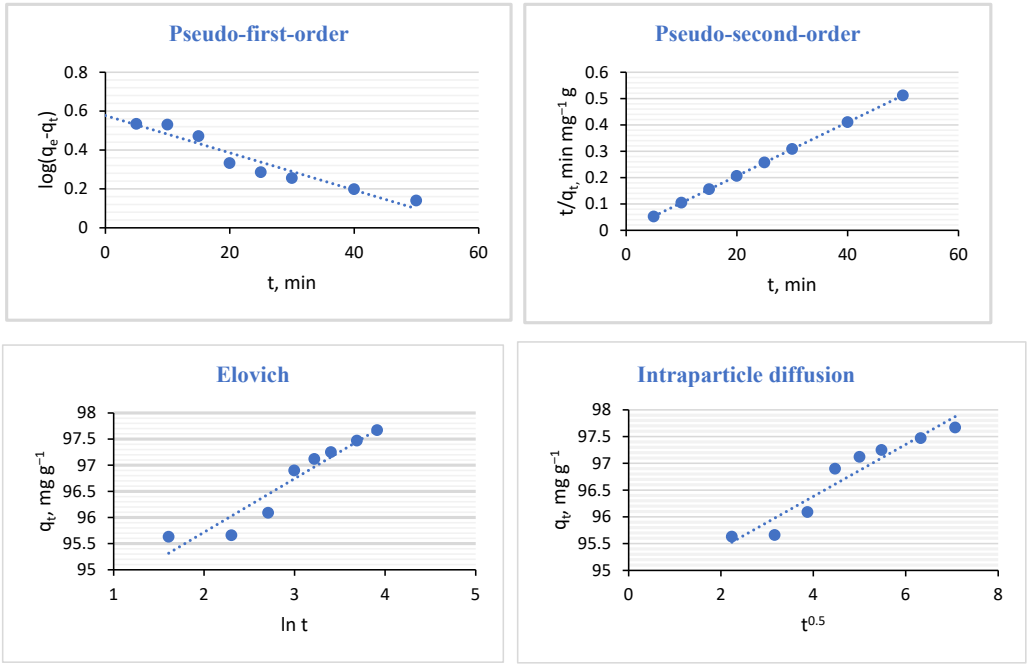


Figure 6. Linear regressions of the plots of the adsorption kinetics of cupric ions by CCs (50 mg of CCs, 50 mL of cupric ion solution (100 mg L^{-1}), temperature of 25 °C, and a solution pH of 6).

2.5. Isotherms of Adsorption

The results of the cupric ions' adsorption isotherms onto CCs are shown in Figure 7, using 10 mg of CCs, a pH of 4, and a temperature of 298 K for 24 h. Table 2 illustrates that the Freundlich isotherm linear plot had a higher R^2 value of 0.960 compared to the Langmuir (0.935), Temkin (0.825), and D-R models (0.919). This indicates that the Freundlich isotherm model is a good fit for the experimental data and is highly effective in explaining the adsorption equilibrium of cupric ions on CCs. It can be deduced that the adsorption process is complex, with multiple layers involved rather than a uniform distribution. Samrot et al. [59] conducted comparable tests with chitosan-coated SPIONs to remove chromium, while Jiang et al. [60] used millimeter-sized magnetic chitosan beads encapsulated with Γ-Fe_2O_3 nanoparticles for Cr(VI) removal from water.

Table 2. Parameters of isotherms of adsorption of cupric ions by CCs.

Models	Parameter	
Langmuir	q_{max}(mg g^{-1})	28.571
	R_L	1.471–0.147
	K_L (L mg^{-1})	0.034
	R^2	0.935
Freundlich	1/n	3.21
	K_f (mg g^{-1})	0.004
	R^2	0.96
Temkin	B (kJ mol^{-1})	238.291
	K_T (L g^{-1})	0.07
	R^2	0.825
D-R	q_m (mg g^{-1})	334.655
	EkJ mol^{-1}	12.504
	B × 10^{-4}	1
	R^2	0.919

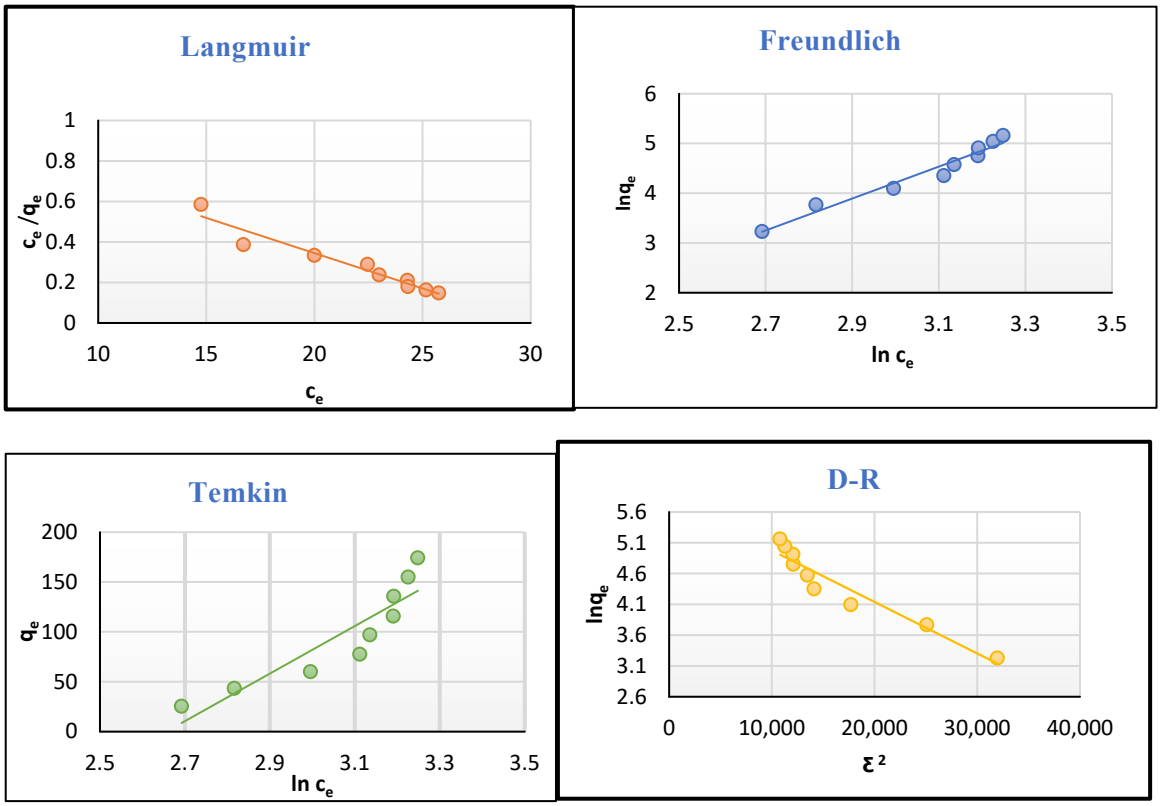


Figure 7. Plots of isotherms of adsorption of cupric ions by CCs (10 mg of CCs, pH 4, temperature of 298 K, 24 h).

2.6. Recyclability of CCs

Subsequent adsorption/desorption cycles were applied to the CCs in order to increase its economic feasibility. Reusing the adsorbent after desorption reduces the funds needed to synthesize new adsorbents [61]. Using HNO_3, the desorption of cupric ions from CCs was performed, and the outcomes are shown in Figure 8. The cupric ion desorption percentages were 77.08, 26.61, 34.61, and 28.32% for four consecutive runs. These results bolster the recycling possibility of CCs and demonstrate that it is a promising adsorbent for eliminating cupric ions from aquatic solutions.

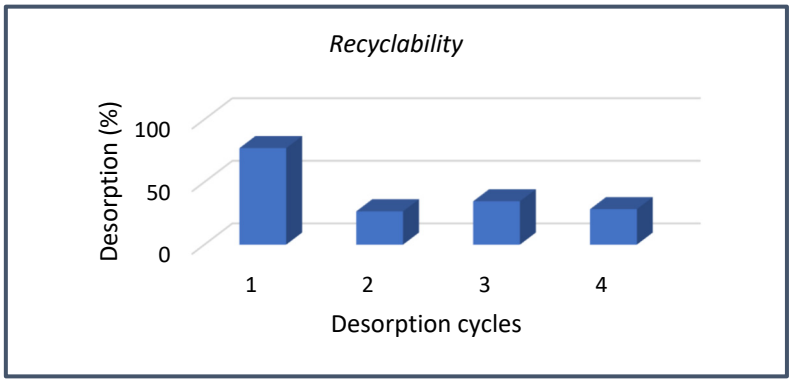


Figure 8. Desorption (%) of cupric ions from CCs.

2.7. Comparation of the Efficiency of Various Materials for Adsorbing Cupric Ions

Table 3 records the adsorbing proficiencies previously reported for some adsorbents for the elimination of cupric ions [40,62–70]. It can be observed that the adsorbing capability of CCs lies in between (larger or smaller) that of those mentioned in Table 3.

Table 3. The q_{max} values of some previously studied adsorbents for the elimination of cupric ions.

Adsorbent	q_{max} (mg g^{-1})	Temperature (°C)	Cupric Ion Conc. (mg L^{-1})	Adsorbent Dose (g)	pH	Ref.
Crosslinked chitosan-g-poly(aniline)	131.58	20–40	100	0.05	6	[40]
Quaternary chitosan microsphere	687.6	25	0–2000	0.075	5	[62]
Calcined horn core	99.98	25	100–500	0.02	5	[63]
Magnetized chitosan/Ag-coated Bi_2WO_6	181.8	20–40	20–120	0.02	6	[64]
Magnetized chitosan modified with xanthate	34.5	25	100	-	5	[65]
Crosslinked chitosan/xanthate with epichlorohydrin	43.47	50	100	-	5	[66]
Medical Salvadora persica plant	74.30	25	100	-	4	[67]
Nutshell of pecan	23.37	30	-	-	5	[68]
H_1	96.20	25	100	0.01	6	[69]
H_2	97.59	25	100	0.01	6	[69]
UCs	99.65	25	100	0.01	6	[70]
CCs	99.05	25	100	0.01	6	Present study

2.8. Adsorption Mechanism

To investigate the mechanism of Cu^{2+} adsorption on CCs, FTIR analysis and computational studies were performed prior to and at the end of Cu^{2+} adsorption. In Figure 9, the FT-IR spectra of CCs and Cu-adsorbed CCs (CCs-Cu) (within the wave number range of 400–4000 cm^{-1}) are depicted. The comparison of the spectra pre- and post-adsorption of copper by CCs revealed clear changes. As is known, the adsorption process is responsible for the deviation phenomenon of the characteristic peaks seen in the spectrum, where Cu(II) heavy metal may chelate with O and/or N atoms to create coordination bonds that alter the electron cloud's density. This ultimately causes a change in the bond's vibrational bands [71]. In the FTIR spectra shown in Figure 9, by comparing the spectra pre- and post-Cu adsorption, it is clear that the highlight with the blue rectangle represents significant changes at the wave numbers ranging from 3200 to 3500 cm^{-1}, corresponding to the N–H and O–H bands on the CCs surface. This indicates that these groups were affected by Cu^{2+} adsorption, confirming their important role in the sorption process. Prior research using pre- and post-adsorption FTIR spectra revealed a large intensity drop of a hydrogen bond at 3500 cm^{-1}, which led Vafakish [72] to discover the coordination interactions between Cu^{2+} and $–NH_2$. Also, similar behaviors were reported by Yin et al. [71].

Before the adsorption of Cu^{2+}, the FTIR spectrum represented that the asymmetric stretching peak of the C=N group in CCs was seen at 1641 cm^{-1}. But, after adsorption, this peak disappeared, which is indicative of the strong interaction of this group in the complexation or electrostatic attraction with Cu^{2+} ions. Further, before the adsorption of Cu^{2+}, the peak of the nitrile group (C≡N) of the cyanoguanidine moiety was seen at 2162 cm^{-1} in the chitosan cyanoguanidine Schiff's base spectra, and a slight decrease in the characteristic peak post-adsorption to 2158 cm^{-1} was noticed, as shown in Figure 9 (marked

with a solid cyan rectangle), reflecting the participation of this group in the complexation with Cu^{2+} ions.

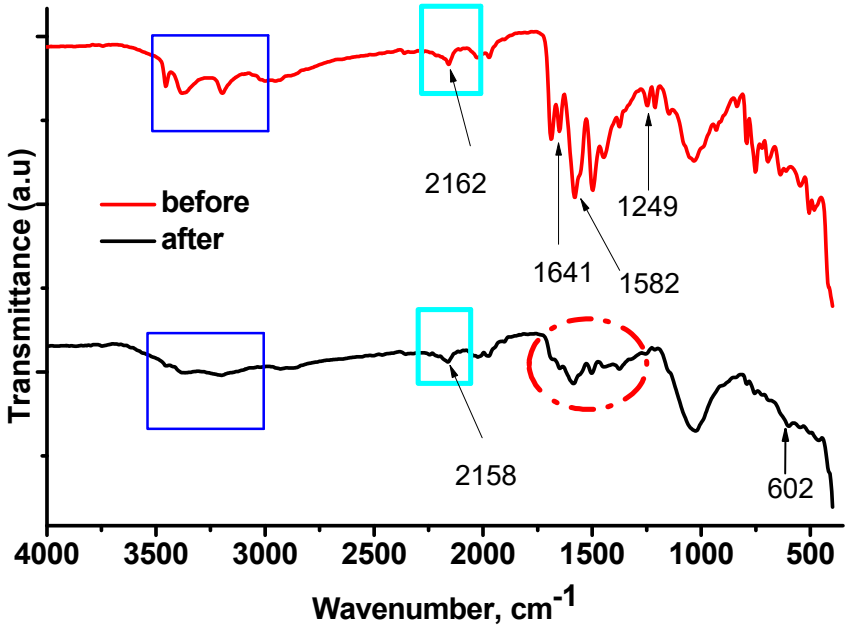


Figure 9. Comparing FTIR spectra of CCs adsorbent before and after Cu^{2+} adsorption.

Additionally, the obvious reductions in intensity at 1582 and 1249 cm^{-1} (marked with a dotted red circle in Figure 9), which correspond to amide II and amide III, respectively, confirmed that nitrogen atoms are the main adsorption sites for copper adsorption on the CCs surface. An additional remarkable band at 602 cm^{-1} was observed in the posterior adsorption FTIR spectrum, which was attributed to the formation of the N-Cu^{2+} bond, wherein cupric and nitrogen lone pairs are shared [72–74]. These outcomes emphasize the important role of the functional groups attached to the cyanoguanidine part, which confirms its effective role in the adsorption process and thus the success of the adsorbent synthesis process.

So, it can be concluded that multiple active centers for the copper adsorption process were observed: the nitrogen and oxygen atoms of the amino and hydroxyl groups in the chitosan part and the nitrogen atoms and hydroxyl groups of attached modifier part. These groups may form surface complexes via direct chelation, ion exchange, and/or electrostatic interaction with Cu(II) as the two principal proposed adsorptive mechanisms.

The latter FTIR analysis results were additionally explored by studying the adsorption mechanism with the following computational study, as shown in Figures 10 and 11 and Table 4. The theoretical binding energy, total energy, and energy gap data of copper ion adsorption onto CCs through different active sites (C≡N, C=N, –NH, $–NH_2$, and –OH) are listed in Table 4. Total energy is a useful metric for assessing whether chemical reactions and stereospecific pathways in intra- and intermolecular processes occur or not, and the system's ground-state energy can be identified by the lowest value of the total energy [75]. Moreover, in order to infer the stability of the adsorbed Cu^{2+} ions at distinct adsorption sites, the binding energy (adsorption energy) E_{ads} of each model is determined [76]. The active sites of the catalyst can be used to anticipate the optimal interaction between it and unacceptable copper wastes. So, we look forward to discovering the lowest total energy and adsorption energy, which will become the most preferable values, being when possible chemical interactions may occur. Consequently, the data collected showed that the calculated E_{ads} and E_T of the undesirable copper ions onto CCs through different proposed active sites reflected the most favorable energetic system for copper adsorption as follows:

C=N > C≡N > –NH_2 > –NH > –OH (Table 4). The obtained results demonstrated the highest negative energy for copper adsorption onto CCs at C=N and C≡N active sites, which was considered as the most favorable energetic system. The explanation for this is that the carbon atoms' electron cloud density increases and the adsorption energy is lowered ("highly negative") due to Cu complexation and the electrical contact that occurs between the contaminant and the nitrogen bound to carbon atoms [77,78].

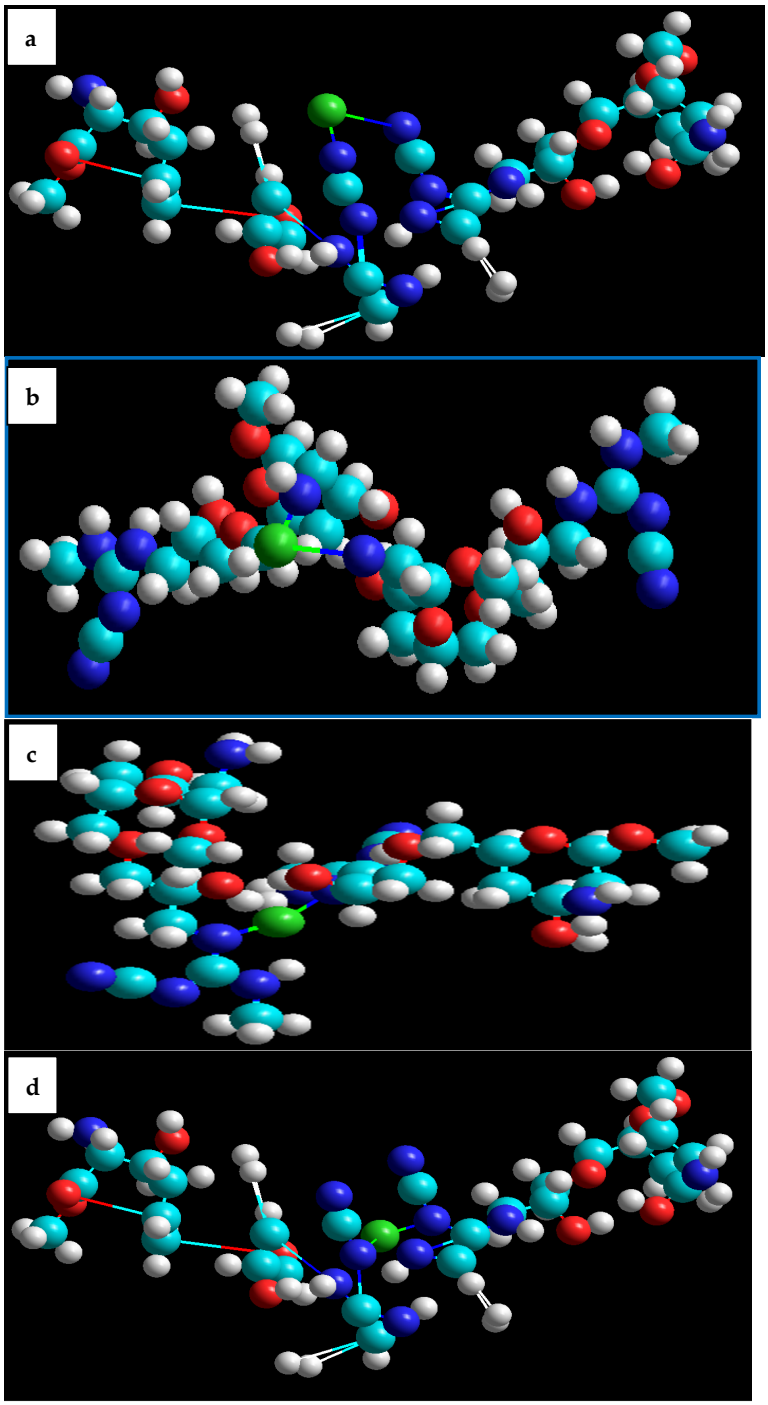


Figure 10. The copper ion interactions with the CCs active sites: (**a**) C≡N, (**b**) –NH_2, (**c**) –NH, and (**d**) C=N. **C; Cu; O; H; N.**

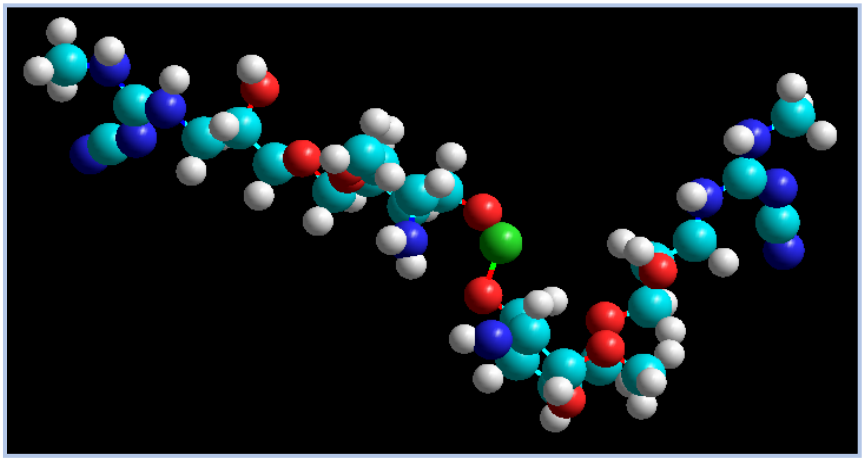


Figure 11. The copper ion interactions with the –OH active site of CCs. **C; Cu; O; H; N.**

Table 4. The total energy (E_T), binding energy (E_{ads}), and energy gap of the adsorbent active sites of CCs and copper.

Active Site	E_T (Kcal/mol)	E_{ads} (Kcal/mol)	E_{HOMO} (ev)	E_{LUMO} (ev)	* Energy Gap (ev)
C=N	−221,601	−9254	−8.09	−0.09	8.00
C≡N	−221,599	−9250	−7.69	−0.68	7.10
$–NH_2$	−220,130	−8989	−8.23	−0.45	7.78
–NH	−220,103	−8961	−8.55	−0.47	8.10
–OH	−220,069	−8928	−5.72	−1.57	4.15

* Energy gap = $E_{LUMO} - E_{HOMO}$ [75].

Also, Table 4 makes it clear that the total energy (E_T) and the E_{ads} of copper adsorbed on –NH and $–NH_2$ active sites are lower than that on the –OH site for CCs demonstrating electron sharing from nitrogen to copper ions [72]. Hence, the interaction that occurred in this instance between the synthetic CCs and the undesired waste was more likely to involve nitrogen sites rather than –OH sites. Furthermore, the resulting complex's E_{gap} between copper ions and CCs through –OH sites was the lowest, indicating that this interaction represented a less stable and more reactive molecule, so this active site interaction is unfavorable. These results validated the cyanoguanidine group's efficacious role in the adsorption process and highlighted the critical importance of the functional groups connected to it. It is worth noting that these outcomes also emphasized the complementarity and consistency between the computed theoretical data and the obtained experimental results (included in the "FTIR results" research section).

Further, the optimum distance between the negative nitrogen in CCs at the $–NH_2$, C≡N, C=N, and –NH active sites and positive copper was determined to be equal to 1.87, 1.83, 1.92, and 1.9Å, respectively (the literature experimental range of Cu–N is 1.95–2.78 Å [79,80]). In contrast, the optimum bond length in the contact between Cu and negative oxygen at the hydroxyl site on the CCs surface was 1.87 Å (the literature experimental range of Cu-O is 1.9–1.92 Å [81]). This decrease in the Cu-N bond or Cu-O length may be due to an increase in the intensity of the contact between copper and nitrogen or oxygen active sites on the CCs surface, and/or electron delocalization. In other words, from the theoretical calculation, the optimized bond length ((Cu-N) and (Cu-O)) for the interaction is lower than the experimental one, indicating that the mechanism may be chemisorption [76].

Recent research using chitosan-based adsorbents has revealed a variety of sorption mechanisms, such as metal ion complexation, electrostatic interactions, surface precip-

itations, ion exchange, etc., for excluding heavy metals such as copper from wastewater [71,78,81]. Taking into account the impact of pH value, the results of the FTIR and computational analyses, and the above adsorption outcomes, the justified mechanisms of cupric adsorbed on CCs are summarized as follows, as depicted in "Figures 10 and 11":

(i) Metal ion complexation is the foremost sorption mechanism to remove Cu^{2+} via CCs through the ion exchange interactions between the protons of functional groups (such as $–NH_2$, C=N, –OH, –NH, etc.) and the Cu^{2+} ions in wastewater.

(ii) These nitrogen atoms function as the main active complexation sites. Taking into account, as theoretically proven, the superiority of nitrogen over oxygen in the complexation process, this may be due to its lower electronegativity than oxygen [74].

(iii) Additionally, it is clear that the ability of Cu^{2+} adsorption by CCs via ion exchange depends on the nature of the functional groups on the adsorbent surface and the pH of the solution. The complex formation occurring between Cu^{2+} and CCs at optimum pH can be expressed as follows:

$$Cu^{2+} + (CCs– NH_3{}^+) + H_2O \leftrightarrow [Cu(CCs– NH_2)]^{2+} + H_3O^+$$

(iv) Electrostatic interaction is another pivotal mechanism for removing copper ions using CCs adsorbents. Therefore, to remove Cu^{+2} ions from wastewater by this mechanism, the adsorbent surface must be negatively charged to cause the attraction of molecules with opposing charges. At pH higher than 6.5, the excessive concentration of negatively charged surface hydroxyl ion functional groups on the adsorbent surface tends to attract copper cations. So, a significant decline in adsorption due to the existence of OH^-, which is more dominant on the adsorbent surface, forms insoluble $Cu(OH)_2$ salts that easily precipitate [78].

(v) In the literature, a significant drop in Cu^{+2} adsorption performance at low pH is reported because the adsorbent surface becomes highly positively charged; so, electrostatic repulsion between cupric ions and the adsorbent surface will occur [70].

Finally, we can conclude that the high removal efficiency of CCs in this study may be attributed to the special presence of several nitrogen and oxygen functional groups on CCs.

3. Experimental

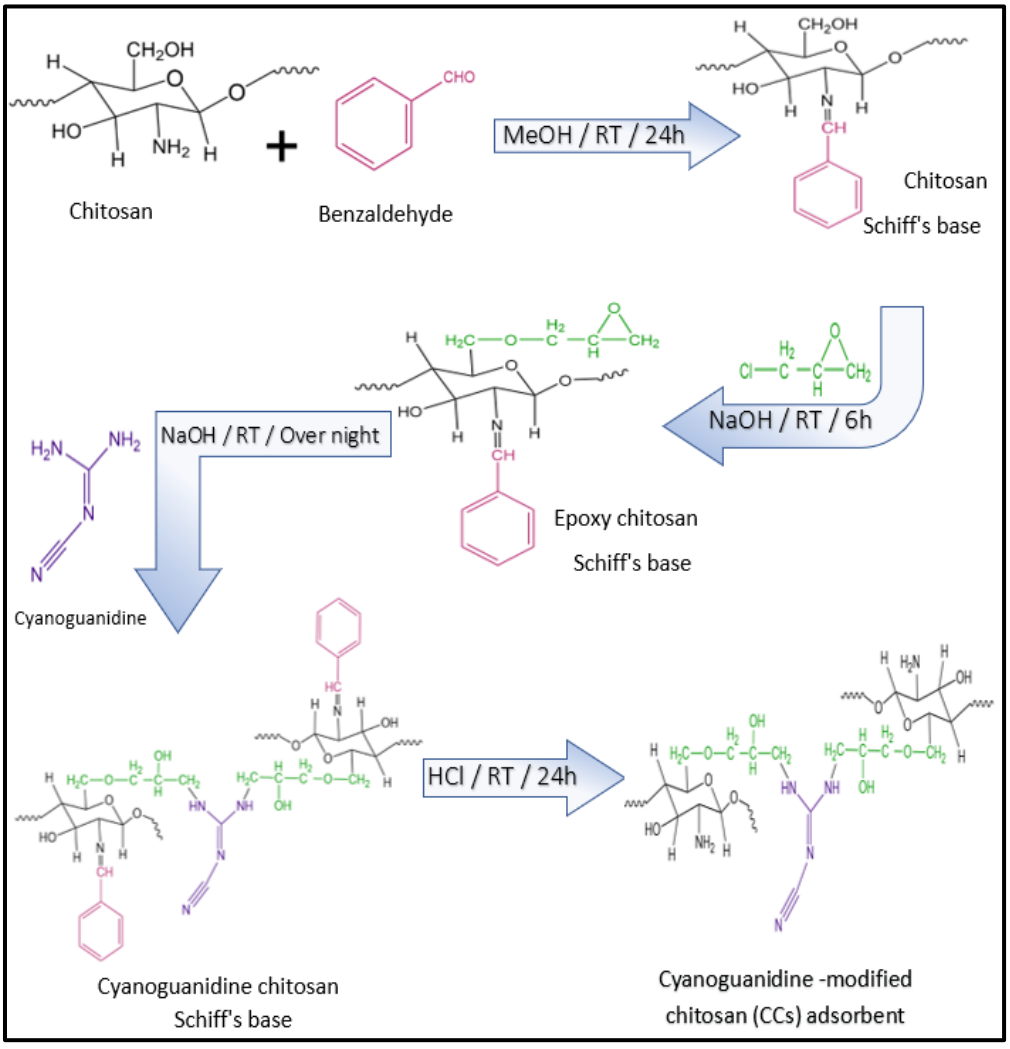
3.1. Materials

Acros Organics (Fairlawn, NJ, USA) provided us with chitosan with a molecular weight of 1.0–3.0 × 10^5 g mol^{-1} and a deacetylation degree of 98%. PanReac. AppliChem-ITW Reagent (Darmstadt, Germany) supplied us with benzaldehyde and epichlorohydrin. Sigma-Aldrich (Munich, Germany) provided us with cyanoguanidine. Merck (Darmstadt, Germany) provided us with $CuSO_4{\cdot}5H_2O$. Sigma-Aldrich (Munich, Germany) was the source of all other chemicals and solvents.

3.2. Synthesis of Cyanoguanidine-Modified Chitosan (CCs) Adsorbent

CCs was synthesized as described in our earlier work [42]. It is necessary to react benzaldehyde with chitosan to protect the amino groups of the latter and consequently direct the chemical change to the -OH groups on C6 of chitosan, which is the first step for creating a chitosan Schiff's base. Twenty milliliters of benzaldehyde was mixed with five grams of chitosan that had been swollen in fifty milliliters of methanol and stirred at 25 °C for twenty-four hours. The formed chitosan Schiff's base was subjected to filtration, washing using MeOH, and drying at 50 degrees Celsius [82]. Second, a suspension of 4 g of the chitosan Schiff's base in 120 mL of a 0.001 mol L^{-1} aqueous NaOH solution was agitated for fifteen minutes at room temperature. Then, 10 milliliters of epichlorohydrin

was introduced into the suspension, followed by six hours of continuous stirring. Then, the crude epoxy chitosan Schiff's base was subjected to filtration, washing several times using water, and drying at 50 degrees Celsius until a constant weight was reached [83]. In the third step, two grams of cyanoguanidine dissolved in twenty-five milliliters of water was added gradually to two grams of epoxy chitosan Schiff's base, which had been swollen in sixty milliliters of aqueous NaOH solution (0.001 mol L^{-1}) and stirred at room temperature for an entire night. The crude cyanoguanidine chitosan Schiff's base was subjected to filtration, washing repeatedly using MeOH and then acetone, and drying at 50 degrees Celsius until a fixed weight was achieved. In the fourth step, 2 g of cyanoguanidine chitosan Schiff's base was mixed with 60 milliliters of ethanol containing hydrochloric acid (0.24 mol L^{-1}), with continuous stirring at 25 °C for twenty-four hours to deprotect the NH_2 groups. The produced cyanoguanidine-modified chitosan (CCs) adsorbent was subjected to neutralization with a 1 wt % aqueous sodium carbonate solution until a pH of 7 was reached; then, it was subjected top filtration, washing using EtOH, and drying at 50 degrees Celsius until a fixed weight was reached (Scheme 2).



Scheme 2. The synthesis of CCs adsorbent (RT = 25 °C).

3.3. Measurements

3.3.1. FTIR Spectroscopy

The modified chitosan derivatives were analyzed using KBr pellets and FTIR spectroscopy on a Thermo Scientific Nicolet 6700 FTIR spectrometer (Yokohama, Japan), with 16 scans in the wavenumber range from 4000 to 400 cm^{-1}.

3.3.2. X-Ray Diffractometry (XRD)

The morphology of the modified chitosan derivatives was investigated using a wide-angle X-ray diffractometer (Rigaku Ultima-IV, Tokyo, Japan) at diffraction angles (2θ) between 5 and 80° at a 5°/min scanning rate.

3.3.3. Scanning Electron Microscopy (SEM)

The SEM images of the surface topography gold-coated modified chitosan derivatives were captured with a field-emission scanning electron microscope JSM-7610F (Jeol, Freising, Germany), using a voltage of acceleration = 15 kV and 8000× magnification.

3.4. Zero Point Charge's pH (pHzpc) Value

CCs (0.1 g) was submerged in a NaCl solution (10 mL, 0.1 M) for 24 h. The pH of the medium was then amended to be in the range 3–11, using aqueous solutions of HCl and NaOH (0.1 N). A Hanna pH meter (Model 211) was used to check the pH value. The value of pHzpc was produced by graphing ΔpH (final pH–initial pH) versus initial pH [47,48].

3.5. Computational Chemistry Analysis

This study used first-principles calculations to theoretically investigate the potential interactions between the synthesized CCs adsorbent and the copper ions. The versatile, sophisticated molecular modeling medium known as HyperChem 8.0 was utilized to calculate each model's total energy (E_T), binding energy (E_{ads}), and geometry optimization.

3.6. Adsorption Investigations

Several tests were carried out to study how cupric ions are absorbed by CCs. Initially, a mixture of 10 mg of adsorbent and 10 mL of the aqueous solution of cupric ions (200–20 mg L^{-1}) was agitated at a specific temperature in a shaker at 80 rpm until equilibrium was achieved. Afterwards, the solution was filtered via 0.45 μm pore size Whatman filter paper, and the copper ion amount was spectrophotometrically determined utilizing an AA-6200 Shimadzu atomic absorption spectrophotometer, Japan.

To study the pH impact, tests of adsorption were performed at different pH values (pH 1–6), employing HCl (0.1 N) while maintaining the rest of the adsorption conditions at similar levels (10 mL of solution of cupric ions (100 mg L^{-1}), CCs (10 mg), 25 °C).

The impact of temperature on the efficiency of adsorption was investigated at various temperatures (25, 35, 45, and 55 °C) while keeping the rest of the adsorption conditions similar (10 mL of solution of cupric ions (100 mg L^{-1}), CCs (10 mg), and pH 4).

The impact of adsorbent quantity was evaluated by carrying out the adsorption procedures, utilizing 2–15 mg of CCs while maintaining the rest of the adsorption conditions at similar levels (10 mL of solution of cupric ions (100 mg L^{-1}), pH of 4, 25 °C).

Equations (1)–(3) can be utilized to determine the amount of cupric ions adsorbed by the adsorbents.

$$q_e = \frac{(C_o - C_e)V}{m} \quad (1)$$

$$q_t = \frac{(C_o - C_t)V}{m} \quad (2)$$

$$\% \text{ Removal efficiency} = \frac{C_o - C_e}{C_o} \times 100 \quad (3)$$

The adsorption capacity at equilibrium is denoted as q_e (mg g^{-1}), and at a certain period of time is symbolized as q_t (mg g^{-1}). C_o is the initial cupric ion concentration prior to soaking of the adsorbent (mg L^{-1}), while C_e signifies the cupric ion concentration at equilibrium (mg L^{-1}). C_t signifies the cupric ion concentration present at a particular time t (mg L^{-1}). V denotes the volume of the solution containing cupric ions in liters, while m is the weight of the adsorbent utilized in grams.

3.7. Adsorption Kinetic Investigations

Studies on the kinetics of adsorption are deemed to be essential to understanding the rate of adsorption because they show the impact of various conditions on the rate of the process. This can be realized via applying models that can characterize this reaction. It also establishes the mechanism of metal ion adsorption by the adsorbing material [84].

The cupric ion adsorption kinetic results were modeled, employing some distinctive models of kinetics, namely pseudo-first-order, Elovich, pseudo-second-order, and intra-particle diffusion models.

3.7.1. Pseudo-First-Order Model

In this model, the liaison between changes in the capacity of adsorption and time is in the order one. Equation (4) states that k_1 represents the rate constant.

$$\frac{dq_t}{dt} = k_1(q_e - q_t) \quad (4)$$

The integration of Equation (4) gives rise to linearized pseudo-first-order Equation (5).

$$\log(q_e - q_t) = \log q_e - \frac{k_1}{2.303}t \quad (5)$$

where k_1 (min^{-1}) and t (min) denote the rate constant of this model and time, respectively. The slope and intercept of the line, obtained from plotting log ($q_e - q_t$) versus t, yield q_e and k_1 values, respectively.

3.7.2. Pseudo-Second-Order Model

Equation (6) represents this model; it shows that the relationship between time and the capacity of adsorption is of the second order. This model proposes that the adsorption of dissolved cupric ions involves chemical sorption through a chemical exchange with the adsorbent surface.

$$\frac{dq_t}{dt} = k_2(q_e - q_t)^2 \quad (6)$$

The linearized state for the pseudo-second-order model, as shown in Equation (7), is yielded via integration with Equation (6).

$$\frac{t}{q_t} = \frac{1}{k_2 q_e^2} + \frac{t}{q_e} \quad (7)$$

where the constant of this model is symbolized as k_2 (g mg^{-1} min^{-1}). The linearized plot of t/qt against t gives q_e and k_2 values for its slope and intercept, respectively.

3.7.3. Model of Elovich

This model is important for describing how activated chemisorption works. It can be utilized to examine the general kinetics of chemisorption, a wide variety of slow adsorption processes, and surfaces of heterogeneous adsorbents. It is expressed by Equation (8).

$$\frac{dq}{dt} = \alpha e^{-\beta q} \tag{8}$$

The integration of the constant rate results in the linearized version, as illustrated in Equation (9).

$$q_t = \frac{1}{\beta}\ln(\alpha\beta) + \frac{1}{\beta}\ln\ t \tag{9}$$

where the rate of the desorption constant is referred to as β (g mg^{-1}), which is related to the coverage of the surface and the chemisorption activation energy. The initial adsorption constant rate is signaled as α (mg g^{-1} min^{-1}). The values of both α and β could be determined from the linear link obtained via plotting q_t versus ln t.

3.7.4. Model of Intraparticle Diffusion

This model was utilized for calculating the rate control of the adsorption, as elucidated in Equations (10) and (11).

$$q_t = (k_{int}\ t^{1/2}) + C \tag{10}$$

$$q_t = (k_{int}\ t^{1/2}) \tag{11}$$

where the constant that is proportional to the thickness of the boundary layer is symbolized as C (mg g^{-1}), while the constant of intraparticle diffusion is denoted as k_{int} (mg g^{-1} $min^{-1/2}$). The values of both C and k_{int} are figured from the intercept and slope of the linear relation, which is yielded via plotting $t_{1/2}$ against q_t.

3.8. Adsorption Isotherms

The fit of the experimental results with some well-known adsorption models was studied to determine the nature of adsorption, the distribution of molecules between the liquid and solid phases, and the interaction between the adsorbate and the adsorbent. The following models were applied: Langmuir, Freundlich, Temkin, and Dubinin–Radushkevich [59].

3.8.1. Langmuir Isotherm Model

This model can be given by Equations (12)–(14).

$$q_e = \frac{q_{max}K_LC_e}{1 + K_LC_e} \tag{12}$$

$$\frac{C_e}{q_e} = \frac{1}{q_{max}K_L} + \frac{C_e}{q_{max}} \tag{13}$$

$$R_L = \frac{1}{(1 + K_LC_o)} \tag{14}$$

where the constant related to the extent of interaction between the adsorbate and the surface of K_L (L mg^{-1}) is symbolized. If the value of K_L is relatively large, this indicates a strong interaction between the adsorbate and adsorbent, while a smaller value implies a weak interaction. The fundamental isotherm property and dimensionless factor (separation factor of Langmuir) is denoted as R_L, and the adsorption capacity of the monolayer is designated as q_{max} (mg g^{-1}). The isotherm characteristics are explicated by R_L, since the isotherm becomes irreversible when $R_L = 0$, favorable when $0 < R_L < 1$, linear when $R_L = 1$, and unfavorable when $R_L > 1$.

3.8.2. Freundlich Isotherm Model

This model can be given by Equations (15) and (16).

$$q_e = K_F C_e^{\frac{1}{n}} \tag{15}$$

$$\ln q_e = \ln K_F + \frac{1}{n} \ln C_e \tag{16}$$

where the experiential constants $1/n$ and K_F are related to the intensity of adsorption and its capacity, respectively.

3.8.3. Temkin Isotherm Model

This model is significant in explaining the interaction between the adsorbent and adsorbate and takes into account various variables. The binding energy is evenly spread out, and the heat of adsorption decreases in a linear fashion once coverage is reached. Equations (17) and (18), depicting this model, are applicable for use.

$$q_e = \frac{RT}{B_T} \ln K_T C_e \tag{17}$$

$$q_e = B_T \text{In} K_T + B_T \text{In}\, C_e \tag{18}$$

where the temperature-controlled Temkin constant is designated as B_T (J mol^{-1}) and the isotherm binding constant of Temkin is denoted as K_T (L g^{-1}). From the slope and intercept, originating from a plot of q_e versus ln C_e, the B_T and K_T constant values are determined, respectively.

3.8.4. Dubinin–Radushkevich (D-R) Isotherm Model

This model is employed for the differentiation of chemisorption and physisorption. The reason behind the development of several layers on microporous adsorbing materials can be understood through it. It is a further general relative to the Langmuir model because it does not assume surface homogeneity. Conversely, inadequate coverage could suggest the adsorbent's variability in surface properties. Equations (19) and (20) represent this model.

$$q_e = q_m \exp^{-\beta \varepsilon 2} \tag{19}$$

$$\text{Ln}\, q_e = \ln (q_m) - \beta \varepsilon^2 \tag{20}$$

Equation (21) could be utilized for calculating ε (Polanyi potential). There is a correlation between ε and the freely mean energy of adsorption for every metallic ion mole when moved to the surface of the adsorbing material. The capacity of saturation by the mono-layer is denoted as q_m (mg g^{-1}).

$$\varepsilon = RT \ln \left(1 + \frac{1}{C_e}\right) \tag{21}$$

where the gas constant R = 8.314 J mol^{-1} K^{-1}, and the absolute temperature is T (K).

β and ln q_m (Equation (20)) values can be obtained via the intercept and slope, respectively, resulting from the plotting between ln q_e and ε^2. Equation (22) can possibly be utilized for calculating the mean free energy.

$$E = (2\beta)^{-0.5} \tag{22}$$

The adsorption is classified as chemisorption when 8 < E < 16 kJ mol^{-1}, whereas it is physisorption when E is lower than 8 kJ mol^{-1} [85].

3.9. Desorption Measurements

The desorption of cupric ions from the adsorbing material was carried out by rinsing it with distilled water to remove the unabsorbed cupric ions, followed by soaking 10 mg of this material in HNO_3 (10 mL, 0.1 M) at room temperature overnight. The quantity of the desorbed cupric ions from the adsorbing material was calculated by applying Equation (23).

$$\% \text{ cupric ions desorption} = q_d/q_a \times 100 \quad (23)$$

where the amounts of cupric ions adsorbed by and desorbed from the adsorbing material are symbolized as q_a and q_d (mg g^{-1}), respectively [23].

4. Conclusions

The current research work was conducted on the purification of industrial wastewater, studying the elimination of cupric ions from water solution using cyanoguanidine-modified chitosan. The findings indicated the powerful ability of cyanoguanidine-modified chitosan to adsorb cupric ions. The Freundlich isotherm and pseudo-second-order models provide a more accurate description of the equilibrium outcomes, indicating that the adsorption process is likely multi-layered in nature. The optimal conditions for removing cupric ions were found to be a pH of 6, a temperature of 25 °C, 200 mg L^{-1} of cupric ions, and 15 mg of CCs. CCs has a removal efficiency of 99.05%. The FTIR results revealed a certain change in distinctive peaks following the adsorption of Cu, indicating functional groups' involvement in the complexation process. The lowest total energy and adsorption energy for Cu adsorption onto CCs were obtained at nitrogen sites rather than OH sites. Obviously, ion exchange, electrostatic attraction, and chelation were the main Cu adsorption mechanisms. The theoretical calculations proved that Cu^{2+} adsorption onto CCs is a chemisorption process. At high pH, a significant drop was revealed in the adsorption due to the precipitation mechanism. Multi-nitrogen and oxygen functional groups on cyanoguanidine-modified chitosan were responsible for its high efficiency. In conclusion, the modification of chitosan by cyanoguanidine showed numerous advantages: (1) it prevented chitosan from solubilizing in acidified solutions (media of adsorption); (2) it introduced nitrogen-plentiful function groups (C=N, C≡N, −NH) that acted as additional active sites for binding cupric ions; and (3) it prevented the expected lessening in the elimination efficiency of cupric ions that generally arises from the consumption of -NH_2 groups of chitosan during modification processes. This represents an eminent practical approach that may promote the development of unique adsorbents for eliminating heavy metals.

Supplementary Materials: The following supporting information can be downloaded at: https://www.mdpi.com/article/10.3390/inorganics13040116/s1, Figure S1: FTIR spectroscopy of chitosan before and after modification; Figure S2: XRD analysis of chitosan before and after modification; Figure S3: SEM analysis of chitosan before and after modification.

Author Contributions: N.A.M. and N.F.A.-H. supervised, conceptualized, and developed the methodology. M.A., S.M.I. and A.e.M.E.M. carried out the investigation. N.A.M., N.F.A.-H., M.A., A.e.M.E.M. and S.M.I. performed the formal analysis and wrote the original draft. N.A.M., N.F.A.-H., M.A. and S.M.I. reviewed and edited the manuscript. All authors have approved the final version for publication. All authors have read and agreed to the published version of the manuscript.

Funding: This research received no external funding.

Data Availability Statement: The data presented in this study are available on request from the corresponding authors.

Acknowledgments: The Researchers would like to thank the Deanship of Graduate Studies and Scientific Research at Qassim University for financial support (QU-APC-2025).

Conflicts of Interest: The authors declare no conflicts of interest.

References

1. Uğurlu, E.; Birol, B.; Gencten, M.; Bayrak, Y. Removal of cupric ions from aqueous solutions by ferrochrome ash: Investigation of mechanism and kinetics. *Water* **2023**, *15*, 1063. [CrossRef]
2. Martins, R.J.E.; Rosana, P.; Rui, A.R.B. Cadmium (II) and zinc (II) adsorption by the aquatic moss Fontinalis antipyretica: Effect of temperature, pH and water hardness. *Water Res.* **2004**, *38*, 693–699. [CrossRef] [PubMed]
3. Renu, M.A.; Kailash, S. Methodologies for removal of heavy metal ions from wastewater: An overview. *Interdiscip. Environ. Rev.* **2017**, *18*, 124–142. [CrossRef]
4. Mohamed, N.A. Novel wholly aromatic polyamide-hydrazides: 6. Dependence of membranes reverse osmosis performance on processing parameters and polymer structural variations. *Polymer* **1997**, *38*, 4705–4713. [CrossRef]
5. Tiravanti, G.; Petruzzelli, D.; Passino, R. Pretreatment of tannery wastewaters by an ion exchange process for Cr(III) removal and recovery. *Water Sci. Technol.* **1997**, *36*, 197–207. [CrossRef]
6. Brooks, C.S. *Metal Recovery from Industrial Waste*; Lewis Publishers Ins.: Portage, MI, USA, 1991; Volume 27.
7. Hu, Z.; Lei, L.; Li, Y.; Ni, Y. Chromium adsorption on high performance activated carbons from aqueous solution. *Sep. Purif. Technol.* **2003**, *31*, 13–18. [CrossRef]
8. da Silva Alves, D.C.; Healy, B.; Pinto, L.A.A.; Cadaval, T.R.S., Jr.; Breslin, C.B. Recent developments in chitosan-based adsorbents for the removal of pollutants from aqueous environments. *Molecules* **2021**, *26*, 594. [CrossRef]
9. Demirbaş, Ö.; Karadağ, A.; Alkan, M.; Doğan, M. Removal of copper ions from aqueous Solutions by hazelnuts. *J. Hazard. Mater.* **2008**, *153*, 677–684. [CrossRef]
10. Elmehbad, N.Y.; Mohamed, N.A. Synthesis, characterization and antimicrobial activity of novel N-acetyl,N′-chitosanacetohydrazide and its metal complexes. *Int. J. Polym. Mater. Polym. Biomater.* **2022**, *71*, 1369–1379. [CrossRef]
11. Lee, H.W.; Cho, H.J.; Yim, J.H.; Kim, J.M.; Jeon, J.K.; Sohn, J.M.; Yoo, K.S.; Kim, S.S.; Park, Y.K. Removal of cupric-ion over amine-functionalized mesoporous silica materials. *J. Ind. Eng. Chem.* **2011**, *17*, 504–509. [CrossRef]
12. Chang, S.H.; Teng, T.T.; Ismail, N. Extraction of Cu (II) from aqueous solutions by vegetable oil-based organic solvents. *J. Hazard. Mater.* **2010**, *181*, 868–872. [CrossRef]
13. Gaetke, L.M.; Chow-Johnson, H.S.; Chow, C.K. Copper: Toxicological relevance and mechanisms. *Arch. Toxicol.* **2014**, *88*, 1929–1938. [CrossRef]
14. Manahan, S.E. *Environmental Chemistry*, 5th ed.; Lewis Publishers: Chelsea, MI, USA, 1991.
15. Atalay, E.; Gode, F.; Sharma, Y.C. Removal of selected toxic metals by a modified adsorbent. *Pract. Period. Hazard. Toxic Radioact. Waste Manag.* **2010**, *14*, 132–138. [CrossRef]
16. Mohamed, N.A. Synthesis, characterization and evaluation of in vitro potential antimicrobial efficiency of new chitosan hydrogels and their CuO nanocomposites. *Int. J. Biol. Macromol.* **2024**, *276*, 133810. [CrossRef] [PubMed]
17. Reza, B.L.; Hamid, R.Z.; Mohammad, E.B. Removal of cupric ions from aqueous solutions by low-cost natural hydroxyapatite/chitosan composite: Equilibrium, kinetic and thermodynamic studies. *J. Taiwan Inst. Chem. Eng.* **2014**, *45*, 1642–1648. [CrossRef]
18. Uchenna, O.; Mamookho, M.; Lukhanyo, M.; Nkemdinma, U.O.; Tendani, S.; Vuyo, M. Toxic metal implications on agricultural soils, plants, animals, aquatic life and human health. *Int. J. Environ. Res. Public Health* **2020**, *17*, 2204. [CrossRef] [PubMed]
19. World Health Organization and United Nations Environment Programme. Health Risks from Marine Pollution in the Mediterranean. Part VII. In *Evaluation of Health Risks from Chemically-Contaminated Seafood*; World Health Organization Regional Office for Europe: Copenhagen, Denmark, 1995.
20. The Council of the European Communities. *Directive 82/176/EEC—On Pollution Caused by Certain Dangerous Substances Discharged into the Aquatic Environment of the Community*; European Union: Brussels, Belgium, 1982.
21. Sahariah, P.; Másson, M. Antimicrobial chitosan and chitosan derivatives. a review of the structure-activity relationship. *Biomacromolecules* **2017**, *13*, 3846–3868. [CrossRef]
22. Mirbagheri, V.S.; Alishahi, A.; Ahmadian, G.; Petroudi, S.H.H.; Omagh, S.M.; Romanize, G. Toward understanding the antibacterial mechanism of chitosan: Experimental approach and in silico analysis. *Food Hydrocoll.* **2024**, *147*, 109382. [CrossRef]
23. Ngah, W.S.; Wan, F.S. Adsorption characterization of Pb (II) and Cu (II) ions onto chitosan-tripolyphosphate beads: Kinetic, equilibrium and thermodynamic studies. *J. Environ. Manag.* **2010**, *91*, 958–969. [CrossRef]
24. Elmehbad, N.Y.; Mohamed, N.A. Terephthalohydrazido cross-linked chitosan hydrogels: Synthesis, characterization and applications. *Int. J. Polym. Mater. Polym. Biomater.* **2022**, *71*, 969–982. [CrossRef]

25. Al-Harby, N.F.; Albahly, E.F.; Mohamed, N.A. Synthesis and characterization of novel uracil-modified chitosan as a promising adsorbent for efficient removal of Congo red dye. *Polymers* **2022**, *14*, 271. [CrossRef] [PubMed]
26. Mohamed, N.A.; Al-Harby, N.F.; Almarshed, M.S. Enhancement of adsorption of Congo red dye onto novel antimicrobial trimellitic anhydride isothiocyanate-cross-linked chitosan hydrogels. *Polym. Bull.* **2022**, *77*, 6135–6160. [CrossRef]
27. Annu, S.; Ahmed, S.; Ikram, S. Chitin and chitosan: History, composition and properties. In *Chitosan: Derivatives, Composites and Applications*; John Wiley & Sons, Inc.: Hoboken, NJ, USA, 2017; pp. 3–24. [CrossRef]
28. Wen, L.; Chen, X.; Chen, C.; Yang, R.; Gong, M.; Zhang, Y.; Fu, Q. Ice-templated porous polymer/UiO-66 monolith for Congo red adsorptive removal. *Arab. J. Chem.* **2020**, *13*, 5669–5678. [CrossRef]
29. Ferfera-Harrar, H.; Benhalima, T.; Lerari, D. Sustainable hydrogel nanocomposites based on grafted chitosan and clay for effective adsorption of cationic dye. *Int. J. Mater. Metallurgical Eng.* **2020**, *14*, 5–15.
30. Alfuraydi, R.T.; Alminderej, F.M.; Mohamed, N.A. Evaluation of antimicrobial and anti-biofilm formation activities of novel poly(vinyl alcohol) hydrogels reinforced with crosslinked chitosan and silver nano-particles. *Polymers* **2022**, *14*, 1619. [CrossRef]
31. Shrestha, R.; Thenissery, A.; Khupse, R.; Rajashekara, G. Strategies for the preparation of chitosan derivatives for antimicrobial, drug delivery, and agricultural applications: A Review. *Molecules* **2023**, *28*, 7659. [CrossRef]
32. Alharbi, R.A.; Alminderej, F.M.; Al-harby, N.F.; Elmehbad, N.Y.; Mohamed, N.A. Design, synthesis, and characterization of novel bis-uracil chitosan hydrogels modified with zinc oxide nanoparticles for boosting their antimicrobial activity. *Polymers* **2023**, *15*, 980. [CrossRef]
33. Woźniak, A.; Biernat, M. Methods for crosslinking and stabilization of chitosan structures for potential medical applications. *J. Bioact. Compat. Polym.* **2022**, *37*, 151–167. [CrossRef]
34. Shanmugapriya, A.; Ramya, R.; Ramasubramaniam, S.; Sudha, P.N. Studies on removal of Cr(VI) and cupric ions using chitosan grafted-polyacrylonitrile. *Arch. Appl. Sci. Res.* **2011**, *3*, 424–435.
35. Xiao, X.; Liang, H.; Chen, W.; Wang, Z. Synthesis and adsorption behavior of chitosan-coated $MnFe_2O_4$ nanoparticles for trace heavy metal ions removal. *Appl. Surf. Sci.* **2013**, *285*, 498–504. [CrossRef]
36. Tonetti, C.; Ferrero, F.; Periolatto, M.; Vineis, C.; Varesano, A.; Mazzuchetti, G. Chitosan coated cotton textiles for copper and chromium ions adsorption. In Proceedings of the XIIIth International Izmir Textile and Apparel Symposium, Izmir, Turkey, 2–5 April 2014; pp. 121–126.
37. Lv, L.; Chen, N.; Feng, C.; Zhanga, J.; Li, M. Heavy metal ions removal from aqueous solution by xanthate-modified cross-linked magnetic chitosan/poly(vinyl alcohol) particle. *RSC Adv.* **2017**, *7*, 27992–28000. [CrossRef]
38. Sutirman, Z.A.; Sanagi, M.M.; Abd Karim, K.J.; Wan, I.W.A.; Hadi, J.B. Equilibrium, kinetic and mechanism studies of cupric and Cd(II) ions adsorption by modified chitosan beads. *Int. J. Biol. Macromol.* **2018**, *116*, 255–263. [CrossRef]
39. Trikkaliotis, D.G.; Christoforidis, A.K.; Mitropoulos, A.C.; Kyzas, G.Z. Adsorption of copper ions onto chitosan/poly(vinyl alcohol) beads functionalized with poly(ethylene glycol). *Carbohydr. Polym.* **2020**, *234*, 115890. [CrossRef] [PubMed]
40. Zare, H.; Taleghanib, H.G.; Khanjani, J. Efficient removal of copper ion from aqueous solution using crosslinked chitosan grafted with polyaniline. *I.J.E. Trans. B Appl.* **2021**, *34*, 305–312. [CrossRef]
41. Ding, Y.; Yang, J.; Cai, J. Preparation of guanidinylated carboxymethyl chitosan and its application in the diffusive gradients in thin films (DGT) technique for measuring labile trace metals in water. *Int. J. Environ. Anal. Chem.* **2018**, *98*, 1275. [CrossRef]
42. Al-Harby, N.F.; Albahly, E.F.; Mohamed, N.A. Kinetics, isotherm and thermodynamic studies for efficient adsorption of Congo Red dye from aqueous solution onto novel cyanoguanidine-modified chitosan adsorbent. *Polymers* **2021**, *13*, 4446. [CrossRef]
43. Raval, N.P.; Shah, P.U.; Ladha, D.G.; Wadhwani, P.M.; Shah, N.K. Comparative study of chitin and chitosan beads for the adsorption of hazardous anionic azo dye Congo red from wastewater. *Desalin. Water Treat.* **2015**, *57*, 1–16. [CrossRef]
44. Yagub, M.T.; Sen, T.K.; Afroze, S.; Ang, H.M. Dye and its removal from aqueous solution by adsorption: A review. *Adv. Colloid Interface Sci.* **2014**, *209*, 172–184. [CrossRef]
45. Wang, L.; Wang, A.-q. Removal of Congo red from aqueous solution using a chitosan/organomontmorillonite nanocomposite. *J. Chem. Technol. Biotechnol.* **2007**, *82*, 711–720. [CrossRef]
46. Alharbi, R.A.; Alminderej, F.M.; Al-Harby, N.F.; Elmehbad, N.Y.; Mohamed, N.A. Preparation and characterization of a new bis-uracil chitosan-based hydrogel as efficient adsorbent for removal of anionic Congo red dye. *Polymers* **2023**, *15*, 1529. [CrossRef]
47. Shukla, K.; Verma, A.; Verma, L.; Rawat, S.; Singh, J. A novel approach to utilize disposable paper cups for the development of adsorbent and its application for the malachite green and rhodamine-B dyes removal from aqueous solutions. *Nat. Environ. Pollut. Technol.* **2020**, *19*, 57–70.
48. Antony, V.S.; Shobana, N.; Durga, S.; Chamarthy, S. Utilization of chitosan-coated superparamagnetic iron oxide nanoparticles for chromium removal. *Appl. Water Sci.* **2018**, *8*, 192. [CrossRef]
49. Taha, A.A.; Ahmed, A.M.; Abdel-Rahman, H.H.; Abouzeid, F.M.; Abdel Maksoud, M.O. Removal of nickel ions by adsorption on nano bentonite: Equilibrium, kinetic and thermodynamics. *J. Dispersion Sci. Technol.* **2017**, *38*, 757–767. [CrossRef]
50. Najim, T.S.; Elais, N.J.; Dawood, A.A. Adsorption of copper and iron using low cost material as adsorbent. *J. Chem.* **2009**, *6*, 161–168. [CrossRef]

51. Hameed, B.H.; Ahmad, A.A. Batch adsorption of methylene blue from aqueous solution by garlic peel, an agricultural waste biomass. *J. Hazard. Mater.* **2009**, *164*, 870–875. [CrossRef] [PubMed]
52. Eskandari, S.; Dong, A.; De Castro, L.T.; Ab Rahman, F.B.; Lipp, J.; Blom, D.A.; Regalbuto, J.R. Pushing the limits of electrostatic adsorption: Charge enhanced dry impregnation of SBA-15. *Catal. Today* **2019**, *338*, 60–71.
53. Gosiaco, P.K.L.; Calvo, L.C.A.L.; Bregente, J.C.; Ponce, M.A.; Sanchez, J.M.P. Biosorption ability of starfruit (*Averrhoa carambola* L.) in removing cadmium and lead in contaminated water samples. *Int. J. Commun. Syst.* **2019**, *7*, 919–923.
54. Esposito, A.; Pagnanelli, F.; Lodi, A.; Solisio, C.; Vegliò, F. Biosorption of heavy metals by sphaerotilus natans: An equilibrium study at different pH and biomass concentrations. *Hydrometallurgy* **2001**, *60*, 129–141. [CrossRef]
55. Babel, S.; Kurniawan, T.A. Cr (VI) removal from synthetic wastewater using coconut shell charcoal and commercial activated carbon modified with oxidizing agents and/or chitosan. *Chemosphere* **2004**, *54*, 951–967. [CrossRef]
56. Mohamed, N.A.; Al-Harby, N.F.; Almarshed, M.S. Effective removal of Basic red 12 dye by novel antimicrobial trimellitic anhydride isothiocyanate-cross linked chitosan hydrogels. *Polym. Polym. Compos.* **2021**, *29*, S274. [CrossRef]
57. Ola, A. Kinetic and isotherm studies of copper (II) removal from wastewater using various adsorbents. *Egypt. J. Aquat. Res.* **2007**, *33*, 125–143.
58. Vijayaraghavan, K.; Teo, T.T.; Balasubramanian, R.; Joshi, U.M. Application of sargassum biomass to remove heavy metal ions from synthetic multimetal solutions and urban storm water runoff. *J. Hazard. Mater.* **2009**, *164*, 1019–1023. [CrossRef] [PubMed]
59. Dash, M.; Chiellini, F.; Ottenbrite, R.M.; Chiellini, E. Chitosan—A versatile semi-synthetic polymer in biomedical applications. *Prog. Polym. Sci.* **2011**, *36*, 981–1014. [CrossRef]
60. Jiang, Y.J.; Yu, X.Y.; Luo, T.; Jia, Y.; Liu, J.H.; Huang, X.J. Γ-Fe_2O_3 nanoparticles encapsulated millimeter-sized magnetic chitosan beads for removal of Cr (VI) from water: Thermodynamics, kinetics, regeneration, and uptake mechanisms. *J. Chem. Eng. Data.* **2013**, *58*, 3142–3149. [CrossRef]
61. Vakili, M.; Zwain, H.M.; Mojiri, A.; Wang, W.; Gholami, F.; Gholami, Z.; Giwa, A.S.; Wang, B.; Cagnetta, G.; Salamatinia, B. Effective Adsorption of Reactive Black 5 onto Hybrid Hexadecylamine Impregnated Chitosan-Powdered Activated Carbon Beads. *Water* **2020**, *12*, 2242. [CrossRef]
62. Cai, L.; Ying, D.; Liang, X.; Zhu, M.; Lin, X.; Xu, Q.; Cai, Z.; Xu, X.; Zhang, L. A novel cationic polyelectrolyte microsphere for ultrafast and ultra-efficient removal of heavy metal ions and dyes. *Chem. Eng. J.* **2021**, *410*, 128404. [CrossRef]
63. Ngueagni, P.T.; Woumfo, E.D.; Kumar, P.S.; Siéwé, M.; Vieillard, J.; Brun, N.; Nkuigue, P.F. Adsorption of cupric ions by modified horn core: Effect of temperature on adsorbent preparation and extended application in river water. *J. Mol. Liq.* **2020**, *298*, 112023. [CrossRef]
64. Yang, L.W.; Qi, P.Y.; Feng, Q.C.; Hua, X.G.; Jie, H.J.; Liang, Z.C.; Lai, B. Enhanced adsorption/photocatalytic removal of cupric from wastewater by a novel magnetic chitosan and bismuth tungstate coated by silver (MCTS-Ag/Bi2WO6) composite. *Chemosphere* **2021**, *263*, 128120. [CrossRef]
65. Zhu, Y.H.; Hu, J.; Wang, J.L. Competitive adsorption of Pb(II), cupric and Zn(II) onto xanthate-modified magnetic chitosan. *J. Hazard. Mater.* **2012**, *221–222*, 155–161. [CrossRef]
66. Kannamba, B.; Reddy, K.L.; AppaRao, B.V. Removal of cupric from aqueous solutions using chemically modified chitosan. *J. Hazard. Mater.* **2010**, *175*, 939–948. [CrossRef]
67. Wahid, F.; Mohammadzai, I.U.; Khan, A.; Shah, Z.; Hassan, W.; Ali, N. Removal of toxic metals with activated carbon prepared from Salvadora persica. *Arab. J. Chem.* **2017**, *10*, 2205–2212. [CrossRef]
68. Aguayo-Villarreal, I.; Muñiz-Valencia, B.P.A.A.R. Preparation of activated carbons from pecan nutshell and their application in the antagonistic adsorption of heavy metal ions. *J. Mol. Liq.* **2017**, *230*, 686–695. [CrossRef]
69. Al-Harby, N.F.; Alrasheedi, M.; Mohammed, A.e.M.E.; Soliman, S.M.A.; Mohamed, N.A. Effective removal of Cu(II) ions from aqueous solution by cross-linked chitosan-based hydrogels. *Water* **2024**, *16*, 2324. [CrossRef]
70. Alrasheedi, M.; Mohammed, A.e.M.E.; Al-harby, N.F.; Khedr, G.E.; Mohamed, N.A. Adsorptive elimination of Cu(II) ions from aqueous solution onto chitosan modified with uracil. *Water* **2024**, *16*, 3695. [CrossRef]
71. Yin, H.; Xiong, Q.; Zhang, M.; Wang, B.; Zhang, F. Multi-principles analysis of cupric adsorption in water on magnetic microspheres and modified chitosan. *J. Environ. Chem. Eng.* **2023**, *11*, 111285. [CrossRef]
72. Vafakish, B.; Wilson, L.D. Cu (II) ion adsorption by aniline grafted chitosan and its responsive fluorescence properties. *Molecules* **2020**, *25*, 1052. [CrossRef]
73. Zhang, H.; Dang, Q.; Liu, C.; Cha, D.; Yu, Z.; Zhu, W.; Fan, B. Uptake of Pb(II) and Cd (II) on chitosan microsphere surface successively grafted by methyl acrylate and diethylenetriamine. *ACS Appl. Mater. Interfaces* **2017**, *9*, 11144–11155. [CrossRef] [PubMed]
74. Mallik, A.K.; Kabir, S.M.F.; Rahman, F.B.A.; Sakib, M.N.; Efty, S.S.; Rahman, M.M. Cupric removal from wastewater using chitosan-based adsorbents: A review. *J. Environ. Chem. Eng.* **2022**, *10*, 108048. [CrossRef]
75. Ibrahim, E.L.S.; Moustafa, H.; El-Molla, S.A.; Abdel Halim, S.; Ibrahim, S.M. Integrated experimental and theoretical insights for Malachite green dye adsorption from wastewater using low cost adsorbent. *Water Sci. Technol.* **2021**, *84*, 3833–3858. [CrossRef]

76. Ibrahim, S.M.; Al-Harby, N.F.; El-Molla, S.A.; Ibrahim, E. New combined Experimental and DFT studies for adsorption of sole Azo- dye and a mixture of two cationic dyes from water on a cheap adsorbent. *Sci. Rep.* **2024**, *14*, 14756. [CrossRef]
77. Huang, J.; Ye, M.; Qu, Y.Q.; Chu, L.F.; Chen, R.; He, Q.Z.; Xu, D.F. Pb (II) removal from aqueous media by EDTA-modified mesoporous silica SBA-15. *J. Colloid Interface Sci.* **2012**, *385*, 137–146. [CrossRef]
78. Sun, X.; Yin, S.; Zhao, L.; Yang, W.; You, Y. Adsorption properties of methylene blue and cupric on magnetically oxidized tannic acid cross-linked carboxymethyl chitosan gels. *Int. J. Biol. Macromol.* **2024**, *278*, 134709. [CrossRef]
79. Hangan, A.C.; Lucaciu, R.L.; Turza, A.; Dican, L.; Sevastre, B.; Páll, E.; Oprean, L.S.; Borodi, G. New copper complexes with antibacterial and cytotoxic activity. *Int. J. Mol. Sci.* **2023**, *24*, 13819. [CrossRef] [PubMed]
80. Valach, F. A bond-valence approach to the semicoordination of copper-oxygen and copper–nitrogen complexes. *Polyhedron* **1999**, *18*, 699–706. [CrossRef]
81. Dev, V.V.; Baburaj, G.; Antony, S.; Arun, V.; Krishnan, K.A. Zwitterion-chitosan bed for the simultaneous immobilization of Zn(II), Cd(II), Pb(II) and cupric from multi-metal aqueous systems. *J. Clean. Prod.* **2020**, *255*, 120309. [CrossRef]
82. Elmehbad, N.Y.; Mohamed, N.A.; Abd El-Ghany, N.A. Evaluation of the antimicrobial and anti-biofilm of novel salicylhydrazido chitosan derivatives impregnated with titanium dioxide nanoparticles. *Int. J. Biol. Macromol.* **2022**, *205*, 719–730. [CrossRef] [PubMed]
83. Elmehbad, N.Y.; Mohamed, N.A.; Abd El-Ghany, N.A.; Abdel-Aziz, M.M. Reinforcement of the antimicrobial activity and biofilm inhibition of novel chitosan-based hydrogels utilizing zinc oxide nanoparticles. *Int. J. Biol. Macromol.* **2023**, *246*, 125582. [CrossRef]
84. Soon, C.Y.; Rahman, N.A.; Tee, Y.B.; Talib, R.A.; Tan, C.H.; Abdan, K.; Chan, E.W.C. Electrospun biocomposite: Nanocellulose and chitosan entrapped within a poly (hydroxyalkanoate) matrix for Congo red removal. *J. Mater. Res. Technol.* **2019**, *8*, 5091–5102. [CrossRef]
85. Alves, D.C.; Coseglio, B.B.; Pinto, L.A.; Cadaval, T.R., Jr. Development of spirulina/chitosan foam adsorbent for phenol adsorption. *J. Mol. Liq.* **2020**, *309*, 113256. [CrossRef]

Disclaimer/Publisher's Note: The statements, opinions and data contained in all publications are solely those of the individual author(s) and contributor(s) and not of MDPI and/or the editor(s). MDPI and/or the editor(s) disclaim responsibility for any injury to people or property resulting from any ideas, methods, instructions or products referred to in the content.